International Journal of Heat and Mass Transfer 52 (2009) 3464–3472

Contents lists available at ScienceDirect

International Journal of Heat and Mass Transfer

journal homepage: www.elsevier.com/locate/ijhmt

Experimental and computational study of constrained melting of phase change materials (PCM) inside a spherical capsule

F.L. Tan [a], S.F. Hosseinizadeh [b,1], J.M. Khodadadi [b,*], Liwu Fan [b]

[a] Nanyang Technological University, School of Mechanical and Aerospace Engineering, 50 Nanyang Avenue, Singapore 639798, Singapore
[b] Mechanical Engineering Department, 270 Ross Hall, Auburn University, AL 36849-5341, USA

ARTICLE INFO

Article history:
Received 23 September 2008
Received in revised form 12 February 2009
Accepted 12 February 2009
Available online 16 April 2009

Keywords:
CFD
Darcy law
Enthalpy method
Melting
Natural convection
Paraffin
PCM
Phase change
Phase change materials
Sphere
Spherical capsule
Thermal energy storage
Thermal instability
Thermal stratification
Visualization

ABSTRACT

An experimental and computational investigation directed at understanding the role of buoyancy-driven convection during constrained melting of phase change materials (PCM) inside a spherical capsule is reported. The computations are based on an iterative, finite-volume numerical procedure that incorporates a single-domain enthalpy formulation for simulation of the phase change phenomenon. A Darcy's Law-type porous media treatment links the effect of phase change on convection. Paraffin wax *n*-octadecane was constrained during melting inside a transparent glass sphere through the use of thermocouples installed inside the sphere. The melting phase front and melting fraction of the PCM are analyzed and compared with numerical solution obtained from the CFD code Fluent. Following a short period of symmetric melting due to prominence of diffusion, expedited phase change in the top region of the sphere and a wavy surface at the bottom of the PCM are observed. The computational predictions point to the strong thermal stratification in the upper half of the sphere that results from rising of the molten liquid along the inner surface of the sphere thus displacing the colder fluid. The waviness and excessive melting of the bottom of the PCM is shown to be underestimated by the experimental observation. This discrepancy is linked to the use of a support structure to hold the sphere. Measured temperature data and computational results near the bottom indicate the establishment of an unstable fluid layer that promotes chaotic fluctuations and is responsible for waviness of the bottom of the PCM. On the other hand, the comparison between the measured and computed temperatures in the top half of the sphere show the stable nature of the molten liquid layer. The computational results start to deviate from the thermocouple readings as one moves lower from the top of the sphere. This delay in predicting the melting instant is linked to the thermal stratification within the "constant temperature bath" that encloses the capsule.

1. Introduction and literature review

Transport phenomena associated with phase change (melting and solidification) plays a key role in a great number of naturally-occurring processes and man-made technologies. In recognition of this, steady progress has been made in gaining a deeper insight into phase change, both from applied and fundamental standpoints. Relevant to the scope of this paper that is related to thermal energy storage systems, a number of studies have focused on melting and solidification of phase change materials (PCM) that are stored within containers of various shapes. Concentrating on melting within spherical capsules, this paper is the outcome of the collaborative experimental and computational work of two research groups that have independently studied phase change in spherical systems. Thus, the relevant studies on phase change (mainly melting) of PCM within spherical capsules are reviewed.

Apart from several analytical reports of diffusion-controlled symmetric phase change processes reported before 1980's – e.g. Grimado and Boley [1] among others – Moore and Bayazitoglu [2] were first to report on the "unconstrained" melting (meaning that the solid portion drops within the melt due to its higher density) of PCM both experimentally and numerically. Assuming that the bottom of the solid region melts so as to remain almost spherical, the polar velocity component within the squeezed gap was approximated as being similar to a pressure-driven flow between parallel plates. The coefficients of the parabolic velocity distribution within the gap were obtained by assuming that the solid and molten shell remains fixed and fluid is injected into the gap to produce the gap flow. The liquid–solid position of the interface and temperature profiles for various Stefan numbers were given at various stages of melting. It was found that within the bulk melt region above the solid, convective currents arising from the dropping of the solid mass generally can not be neglected. Bahrami

* Corresponding author. Tel.: +1 334 844 3333; fax: +1 334 844 3307.
E-mail address: khodajm@auburn.edu (J.M. Khodadadi).
[1] Currently Assistant Professor, Mechanical Engineering Department, Babol Noshirvani University of Technology, I. R. Iran.

0017-9310/$ - see front matter © 2009 Elsevier Ltd. All rights reserved.
doi:10.1016/j.ijheatmasstransfer.2009.02.043

Nomenclature

c_p	constant pressure specific heat (J/kg K)
C	porosity constant (kg/m^3 s)
L	latent heat of fusion (J/kg)
Pr	Prandtl number, defined as ν/α
R	inner radius of the spherical capsule (m)
Ra	Rayleigh number, defined as $8g\beta(T_0 - T_m)R^3/\nu\alpha$
Ste	Stefan number defined as $c_p(T_0 - T_m)/L$
t	time (s)
T	temperature of the PCM (K)
T_i	initial temperature of the PCM (K)
T_m	melting temperature of the PCM (K)
T_0	surface temperature of the capsule (K)
V_r	radial velocity component (m/s)
V_θ	polar velocity component (m/s)
Greeks	
α	thermal diffusivity (m^2/s)
β	thermal expansion coefficient (K^{-1})
λ	liquid volume fraction
ν	kinematic viscosity (m^2/s)

and Wang [3] also investigated the "unconstrained" melting process in a sphere. Assuming pressure-driven flow between parallel plates as the prevailing gap condition, the corresponding velocity distribution was obtained. Considering diffusion-controlled heat transfer to the melting front and decoupling of the temperature and velocity fields, an approximate closed-form expression for the melting process was derived and the dependence of the interface properties on time was elucidated. Following along the lines of [2,3], Roy and Sengupta [4] reported an analytical solution for the melting rate on the bottom surface of the solid core. The effect of the solid phase uniformly subcooled at the outset was investigated by Roy and Sengupta [5]. Due to accounting for the temperature gradient in the solid core, closed-form analytic solution was not plausible and a numerical approach was adopted. If the degree of subcooling was raised above 0.5, the melt rate was observed to slow down markedly and more uniform variation of the Nusselt number on the lower surface of the sphere was obtained. It is noteworthy to mention that convection considered in [2–5] is due to squeezing of the solid core against a thin liquid layer. The effect of natural convection within the thin melting layer in the bottom of the sphere and within the top part of the sphere during the unconstrained melting process was studied by Roy and Sengupta [6]. The two zones were analyzed independently with appropriate coupling conditions utilized at the liquid–solid interface. They reported that marked melting took place at the upper surface due to the significance of natural convection, whereas in previous research [2–5], the effect of natural convection on the melting process was neglected. Fomin and Saitoh [7] outlined an approximate mathematical model of contact melting of an unconstrained solid in a spherical capsule with a non-isothermal wall. Employing the perturbation method, closed-form analytical expressions for the thickness of the molten layer, melting rate and melting time were obtained. These were then found to be in good agreement with numerical solution of the complete equations for their model. Cho and Choi [8] reported temperature readings within spherical capsules that contained *n*-tetradecane and a mixture of *n*-tetradecane (40%) and *n*-hexadecane (60%) and water. The capsules made up a 7-layer thermal storage system. The constrained melting and freezing periods for various PCM and position of the capsule within the thermal storage system were reported. Khodadadi and Zhang [9] reported their finite-volume-based computational study of the effects of buoyancy-driven convection during melting of "constrained" PCM within spherical containers. Phase change and its effect on convection were modeled via a single-domain enthalpy formulation and a Darcy's law-type porous media treatment, respectively. As buoyancy-driven convection became more dominant due to the growth of the melt zone, accelerated melting in the top region of the sphere in comparison to the bottom zone was observed. When buoyancy effects were very marked, as many as three time-dependent recirculating vortices were observed. The computational findings were verified through qualitative constrained melting experiments using a high-Prandtl number wax. Eames and Adref [10] investigated experimentally the freezing and melting processes for water contained in spherical enclosures. Semi-empirical relations for the instantaneous mass of ice within a sphere were provided and a novel method to trace the water–ice interface position during the freezing process was outlined. Further information of their experimental findings [10] was reported by Adref and Eames [11]. A combination of experimental and diffusion-based theoretical findings addressing formation of ice inside a spherical capsule was reported by Ismail et al. [12]. The effects of the shell material/thickness, initial subcooling and external temperature were studied. By providing visualization photographs, Koizumi [13] communicated limited results of an experimental study of constrained melting of PCM within spherical capsules that were placed in a controlled flow stream. Ettouney et al. [14] refer to literature that discuss utilization of spherical PCM capsules in storage systems and disregarded earlier work that has been discussed so far here. They performed both melting and solidification experiments of commercial grade paraffin wax within copper spherical capsules. The capsules were instrumented with 10 thermocouples placed along two axes normal to each other, thus constituting a constrained melting condition. For melting of the PCM, the capsule was heated by an air stream flowing vertically upward within a tube. No flow visualization photos were possible in this arrangement and liquid–solid interfaces could only be inferred from the thermocouple readings. Regin et al. [15] discussed an experimental and numerical study of a spherical capsule filled with paraffin wax (melting temperature range of 52.9–61.6 °C) as the constrained PCM and placed in a convective environment during the melting process. Time-resolved temperature readings were obtained using a rake of nine thermocouples that were placed on a horizontal plane passing through the center of the sphere. Keeping the initial temperature of the PCM constant, the temperature of the convective heat transfer fluid was varied from 70 to 82 °C corresponding to Stefan numbers of 0.1143–0.2501. A diffusion-only 1D model for phase change using the enthalpy method and finite difference formulation was developed. The model was then used to investigate the effect of capsule size and the Stefan number on the instantaneous heat flux, liquid fraction and melting time. Unconstrained melting of the R27 paraffin wax in a spherical geometry was explored numerically and experimentally through visualization by Assis et al. [16]. Convection within the liquid phase, volumetric expansion induced by melting, sinking of the solid, and close contact melting phenomenon were incorporated in the simulations. The numerical results compared favorably to the experimental findings. Mean Nusselt numbers and melt fractions were related to the Fourier, Stefan, and Grashof groupings. Both constrained and unconstrained melting of *n*-octadecane inside spheres were investigated by Tan [17]. Various combinations of

the initial subcooling and wall temperatures were considered. In addition to providing flow visualization photographs, temperature measurements were collected. The detailed temperature recordings for the constrained melting part of that study [17] are used for comparison against the computational results in the present study. Efforts directed at unifying analytic techniques similar to [2–5,7] in order to generalize unconstrained (also termed contact) melting of PCM within symmetric enclosures are still pursued [18]. The generalized analysis that led to mathematical expressions of the film thickness, rate of melting, elapsed time period to complete melting, and Nusselt number was then applied to specific problems of contact melting inside cylindrical and elliptical tubes, as well as the spherical capsule. It should be noted that the melting problem in a horizontal cylindrical capsule shares many of the features discussed in this paper. The interested reader is referred to [19,20].

In extending the knowledge base on constrained melting in a sphere and its relation to buoyancy-driven convection [8,9,13–15,17] a combined experimental/computational study was undertaken. Predictive capabilities of a commercial CFD code that utilizes a single-domain enthalpy formulation were tested against detailed flow visualization and thermocouple measurements inside a transparent glass sphere. In addition to the novelty of the approach, the strong presence of an expected unstable flow structure at the bottom of the sphere and its effect on the waviness and enhanced melting of the solid PCM is uncovered.

2. Physical and mathematical models

The problem to be considered is that of a spherical capsule (inner radius R and a finite wall thickness) that initially holds a solid PCM at temperature T_i that may be lower than the melting temperature (T_m), i.e. the phase change material could be *subcooled*. At time $t > 0$, the outer surface of the capsule is held at a constant temperature (T_0), such that $T_0 > T_m$. Heat is conducted through the wall of the capsule, causing the PCM to start to melt next to the inner surface of the capsule. Similar to prior work of the authors [9,17] and others [8,13–15] focus of this paper will be on constrained melting. This means that density differences of the liquid and solid phases are neglected in the mathematical simulations, thus dropping of the heavier solid PCM is not treated. Experimentally, falling of the solid PCM is inhibited by its adherence to a rake of thermocouples that will also serve as sensors of the instantaneous temperatures within both solid and liquid phases. The pertinent details of the experimental set-up and the mathematical model that were used to simulate this melting process are outlined next

2.1. Experimental set-up

Detailed discussion of the experimental set-up is provided elsewhere [17]. The main component of the experiment was a spherical glass capsule within which the PCM was contained. Paraffin wax *n*-octadecane was used as the PCM and its thermophysical properties are summarized in Table 1. A schematic drawing of the spherical capsule and its pertinent dimensions are given in Fig. 1, where the locations of 11 type-K thermocouples are identified. Eight thermocouples, identified as A through H, were placed vertically along the symmetry axis that passed through the center of the sphere. Thermocouple E was at the center of the sphere and the respective locations of the other seven thermocouples are given in Table 2. Three other thermocouples identified as I, J, and K had the same elevations as thermocouple E but were used to monitor the temperatures next to the glass wall inside and outside the capsule. Initially, the capsule was filled with the liquid PCM and allowed to solidify inside a freezer, thus achieving a certain degree of subcooling. The spherical capsule was then lowered into the middle of a Plexiglas water tank, through which hot water originating from a bath circulator was circulated [17]. For the experimental data presented here, the solid was subcooled to 1 °C and the temperature of the surface of the sphere was maintained at 40 °C. The pertinent Prandtl, Rayleigh, and Stefan numbers for the problem at hand were 59.5, 2.63×10^8, and 0.113, respectively. Some measurements with subcooling of 10 and 20 °C were also reported by Tan [17].

Table 1
Thermophysical properties of *n*-octadecane.

Melting temperature	28.2 °C
Density	772 kg/m^3
Kinematic viscosity	5×10^{-6} m^2/s
Specific heat	2330 J/kg K
Thermal conductivity	0.1505 W/m K
Latent heat of fusion	243.5 kJ/kg
Thermal expansion coefficient	0.00091 K^{-1}

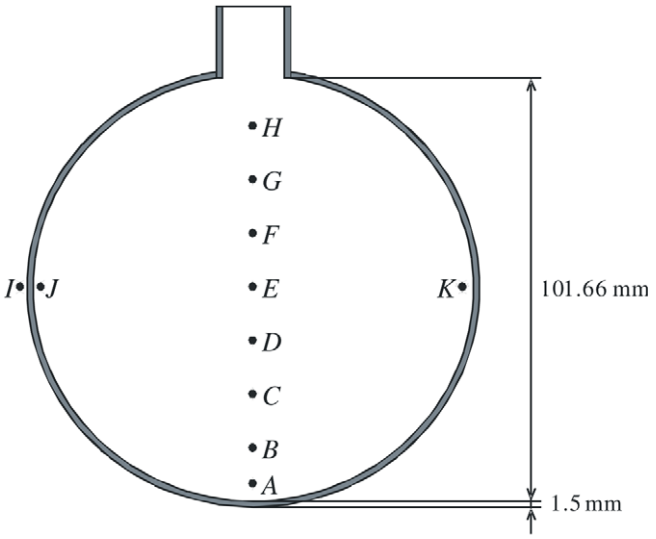

Fig. 1. Schematic diagram of the spherical capsule and locations of the thermocouples.

2.2. Governing equations

In light of the constrained melting requirement for the PCM, the pertinent assumptions are:

1. Both the liquid and solid phases are isotropic and homogeneous, thus their thermophysical properties are taken to be constants.
2. The melting of the PCM will be axisymmetric.
3. The two phases at the liquid–solid interface remain in thermal equilibrium (T_m).
4. The density change within the liquid phase that drives natural convection is only considered in the body force terms (Boussinesq approximation).

Based on the foregoing assumptions, the governing equations in the spherical coordinates (r and θ being the radial and polar coordinates, respectively) are:

Continuity:

$$\frac{1}{r^2}\frac{\partial}{\partial r}(V_r r^2) + \frac{1}{r\sin\theta}\frac{\partial}{\partial \theta}(V_\theta \sin\theta) = 0. \quad (1)$$

Table 2
Time instants of phase change along the rake of thermocouples.

	Point and its distance (mm)							
	A	H	G	B	F	E	C	D
Above* or below* center	−44	+37.5	+25	−37.5	+12.5	0	−25	−12.5
Experiment (min)	6	26	44	68	78	104	122	126
Computation (min)	16	24	42	32	56	68	84	82

* + and − values indicate above and below the center of sphere, respectively.

Polar direction momentum:

$$\frac{\partial V_\theta}{\partial t}+\frac{1}{r^2}\frac{\partial}{\partial r}(V_r r^2 V_\theta)+\frac{1}{r\sin\theta}\frac{\partial}{\partial\theta}(V_\theta \sin\theta V_\theta) = \nu\left(\frac{1}{r^2}\frac{\partial}{\partial r}\left(r^2\frac{\partial V_\theta}{\partial r}\right)+\frac{1}{r^2\sin\theta}\frac{\partial}{\partial\theta}\left(\sin\theta\frac{\partial V_\theta}{\partial\theta}\right)\right)-\frac{1}{\rho}\frac{1}{r}\frac{\partial p}{\partial\theta} - g\beta(T-T_m)\sin\theta-\frac{V_r V_\theta}{r}+\nu\frac{2}{r^2}\frac{\partial V_r}{\partial\theta}-\frac{\nu}{r^2\sin^2\theta}V_\theta-\frac{C(1-\lambda)^2}{\rho\lambda^3}V_\theta. \quad (2)$$

Radial direction momentum:

$$\frac{\partial V_r}{\partial t}+\frac{1}{r^2}\frac{\partial}{\partial r}(V_r r^2 V_r)+\frac{1}{r\sin\theta}\frac{\partial}{\partial\theta}(V_\theta \sin\theta V_r) = \nu\left(\frac{1}{r^2}\frac{\partial}{\partial r}\left(r^2\frac{\partial V_r}{\partial r}\right)+\frac{1}{r^2\sin\theta}\frac{\partial}{\partial\theta}\left(\sin\theta\frac{\partial V_r}{\partial\theta}\right)\right)-\frac{1}{\rho}\frac{\partial p}{\partial r} + g\beta(T-T_m)\cos\theta+\frac{V_\theta^2}{r}-\nu\frac{2}{r^2}\frac{\partial V_\theta}{\partial\theta}-\nu\frac{2\cot\theta}{r^2}V_\theta-2\frac{\nu}{r^2}V_r-\frac{C(1-\lambda)^2}{\rho\lambda^3}V_r. \quad (3)$$

Thermal energy equation:

$$\frac{\partial H}{\partial t}+\frac{1}{r^2}\frac{\partial}{\partial r}(V_r r^2 H)+\frac{1}{r\sin\theta}\frac{\partial}{\partial\theta}(V_\theta \sin\theta H) = \frac{k}{\rho c_p}\left(\frac{1}{r^2}\frac{\partial}{\partial r}\left(r^2\frac{\partial H}{\partial r}\right)+\frac{1}{r^2\sin\theta}\frac{\partial}{\partial\theta}\left(\sin\theta\frac{\partial H}{\partial\theta}\right)\right) - \frac{1}{\rho c_P}\left(\frac{\partial(\Delta H)}{\partial t}+\frac{1}{r^2}\frac{\partial}{\partial r}(r^2 V_r \Delta H)+\frac{1}{r\sin\theta}\frac{\partial}{\partial\theta}(V_\theta \Delta H\sin\theta)\right). \quad (4)$$

The *enthalpy formulation* that is utilized here belongs to the single-region (or continuum) class of available methods. The source term for the thermal energy equation (last three terms on the right-hand side of Eq. (4)) can be derived by splitting the total enthalpy of the material into its sensible enthalpy ($H = c_p T$) and latent heat (ΔH) [21]. The relation between the latent heat and temperature was assumed to be linear [9]. This single-domain enthalpy–porosity formulation treats different phases as porous media. In effect, Darcy Law damping terms of the form $\frac{C(1-\lambda)^2}{\lambda^3}V_i$ with $i = r$ and θ were added to the momentum equations to account for the effect of phase change on convection. These Darcy damping terms will conveniently force the velocity in the solid phase to zero. The term λ stands for the liquid volume fraction at a given point (i.e. unity for the liquid phase or zero for the solid phase). The mushy zone constant (C) was set to 10^5 kg/m^3 s. Due to our focus on phase change of a pure material, the last two components of the source term of the thermal energy equation were neglected. This is justified since ΔH is constant in the solid and liquid phases, thus making the two terms negligible due to mass conservation. Khodadadi and Zhang [9] provided the dimensionless form of the governing equations, showing that the Prandtl, Rayleigh, Stefan, Subcooling, and Darcy groupings are the parameters that govern this problem.

2.3. Computational methodology

The SIMPLE method [22] within version 6.2.16 of the commercial code FLUENT [23] was utilized for solving the governing equations. A grid system of 7636 triangular and quadrilateral cells was found to be sufficient to resolve the details of the flow and temperature fields based on comparison of the streamline contours and liquid–solid interface positions for various grid densities. Adoption of fine grid distribution in the radial direction allowed the use of longer time steps. The time step for integrating the temporal derivatives was set to 0.1 s, following comparison of selected quantities obtained from simulations using 1, 0.5, 0.1, 0.05, and 0.01 s. The Power Law differencing scheme was used for solving the momentum and energy equations, whereas the PRESTO scheme was adopted for the pressure correction equation. The under-relaxation factors for the velocity components, pressure correction, thermal energy, and liquid fraction were 0.3, 0.1, 1, and 0.9, respectively. In order to satisfy convergence criteria (10^{-6}), the number of iterations for every time step was between 200 and 400.

2.4. Boundary and initial conditions

Given the availability of a thermocouple reading (I) on the outer surface of the sphere that remained fairly constant [17] a constant temperature was imposed on the outer surface of the spherical capsule. FLUENT then solved a 1D conduction equation to assign the temperature of the inside wall where the no slip boundary condition for the two velocity components was enforced. At time $t = 0$, the PCM is taken to be a motionless solid that is maintained at a constant temperature 1 °C below the melting temperature, of the PCM.

3. Results and discussion

Qualitative observations of the phase change patterns during constrained melting of the PCM that were afforded by the visualization of the melting patterns are discussed first. These observations will then be linked to quantitative results of CFD simulations and detailed thermocouple readings.

3.1. Flow visualization of the melting patterns

The solid–liquid fronts for the constrained melting of the PCM within the spherical capsule after 0, 20, 40, 60, 80, 100, and 120 min are shown in Fig. 2. The solid was subcooled to 1 °C below the melting temperature of the paraffin *n*-octadecane (28.2 °C) and the surface temperature of the sphere was maintained at 40 °C. Tan [17] presented similar photographs at various time instants for the case with a 10 °C subcooling. In combination, photographs of Fig. 2 and those provided by Tan [17] provide a detailed history of the constrained melting within a spherical capsule. Due to the low value of subcooling, the solid PCM is quickly wrapped in a very thin liquid film early on. This is clearly observed in the photograph that was taken after 20 min. Melting of the solid PCM continues and photographs taken after 40 and 60 min exhibit more intense melting in the upper zone in comparison to the side and bottom sections. In the absence of a "squeezed" film layer associated with unconstrained melting [2–7,17,18] that primes convective liquid motion toward the top of the sphere, thus masking the true contribution of buoy-

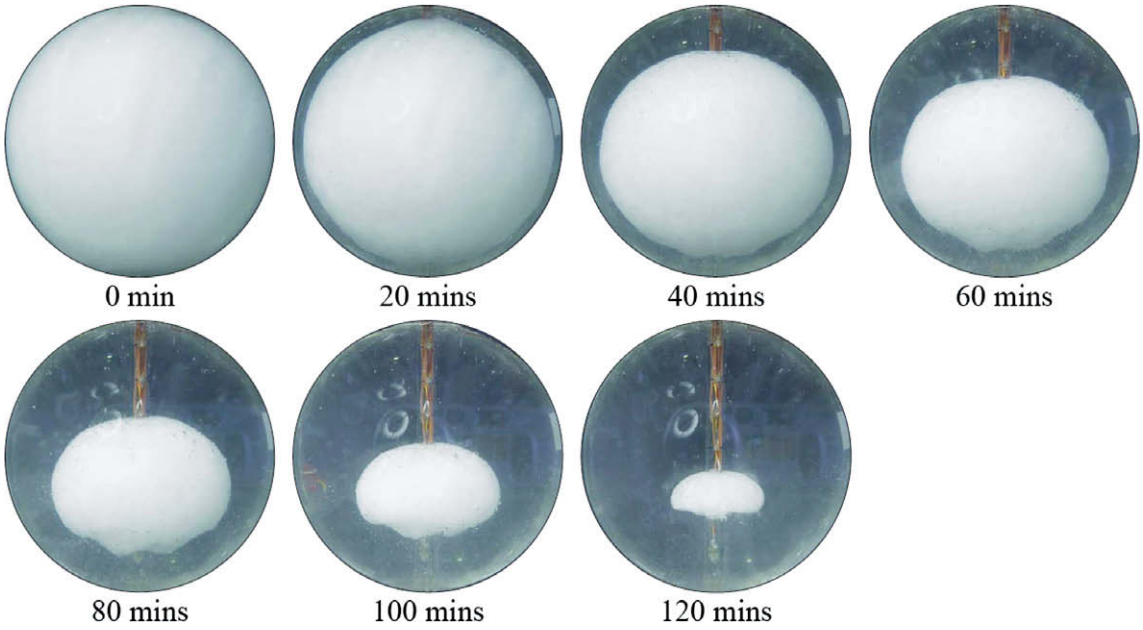

Fig. 2. Instantaneous photographs of the melting of PCM inside the spherical capsule after 0, 20, 40, 60, 80, 100, and 120 min.

ancy-driven convection, Khodadadi and Zhang [9] attributed this preferred zone of melting to the strong role of natural convection in the upper region of the sphere. In short, the molten liquid between the inner wall of the capsule and the solid PCM rises upward along the glass wall thus replacing the colder liquid that moves downward along the solid PCM. The oblate shape of the solid PCM in the photographs taken after 80 and 100 min is distinctly indicative of the intensity of buoyancy-driven convection responsible for expedited melting in the top zone. Another interesting observation has to do with the waviness of the surface at the bottom of the solid PCM. This phenomenon is observed in the photographs taken after 60, 80, and 100 min and this will be discussed in greater detail below.

3.2. Time-dependent flow structures, temperature fields, and liquid fraction

The instantaneous contours of the streamlines and colorized temperature fields after 10, 20, 30, 40, 50, 60, 70, 80, and 90 min following commencement of heating are given in Fig. 3. The streamlines are drawn on the left half of each circle, whereas the colorized temperature contours are shown on the right half. At a given instant during the melting process, the dark blue [only available in the downloadable version of the paper] portion of the temperature contours that occupy the center of the sphere indicates the unmelted solid phase. In the absence of convection, diffusion-controlled melting would have caused the unmelted PCM to remain a perfect sphere at all times [1 and others before them] and concentric temperature contours will have been observed at every instant during the melting process. However, upon quick melting of the PCM next to the inner wall of the sphere, the hot liquid film next to the wall rises upward, thus absorbing more heat during its travel to the top of the sphere. During this process, the colder fluid at the top is bound to be displaced downward along the surface of the solid PCM. Thus, a recirculating vortex is formed between the solid PCM and the inner wall of the sphere that is clearly observed at the 10, 20, and 30 min instances. Naturally, the size of this vortex will increase as the PCM melts further. Even though the spherical shape of the solid PCM is preserved well within 30 min into the process, temperature contours of Fig. 3 distinctly show that the thermal field is far different than the limiting diffusion-controlled melting phenomenon. With the hot liquid occupying the top portion of the sphere, thermal stratification is well underway. The reader is also directed to note the strong buoyancy-driven convection near the very bottom of the sphere within the first 30 min. Within that zone, an unstable convection layer has been formed thus leading to easy lifting of the hot fluid parallel to the vertical axis. At the 20-min instant, a small recirculating zone is observed at the bottom of the sphere. This will be discussed later in connection with the stable/unstable layers. Between the time instants of 40 and 60 min, due to the short proximity of the stratified hot liquid, noticeable melting takes place in the top portion of the solid PCM. However, the more interesting observation within this time period is the intense waviness of the bottom of the solid PCM followed by its expedited melting, as if a hot liquid jet was drilling into the bottom of the solid PCM. This observation on waviness was also observed in the flow visualization photographs of Fig. 2 and it will be explained later on in Section 3.4. At the 70th minute, the highest point of the solid (20% of the original PCM at this instant) coincides with the center of the sphere, thus clearly pointing to the preferential melting pattern in the top half of the sphere. By the 80th minute, the solid PCM is a dome-shaped solid with top and bottom concave-down surfaces. By the 90th minute, the sphere is completely filled with molten liquid and a fully stratified spherical container is at hand. From this point forward, transient natural convection is the prevailing phenomenon that has also been studied by the authors, e.g. Zhang et al. [24] and Duan et al. [25].

The instantaneous values of the liquid fraction within the spherical capsule that were determined both computationally and experimentally are compared in Fig. 4. Even though the computational technique captures the trends of the constrained melting of a sphere, it predicts a faster rate of melting. The experimental data were determined through the use of solid modeling obtained from digitizing the solid–liquid interface of the photographs in Fig. 2 and its details are discussed by Tan [17]. Thus, one should note that there is a possibility of three-dimensional melting effects that were not accounted for in this analysis.

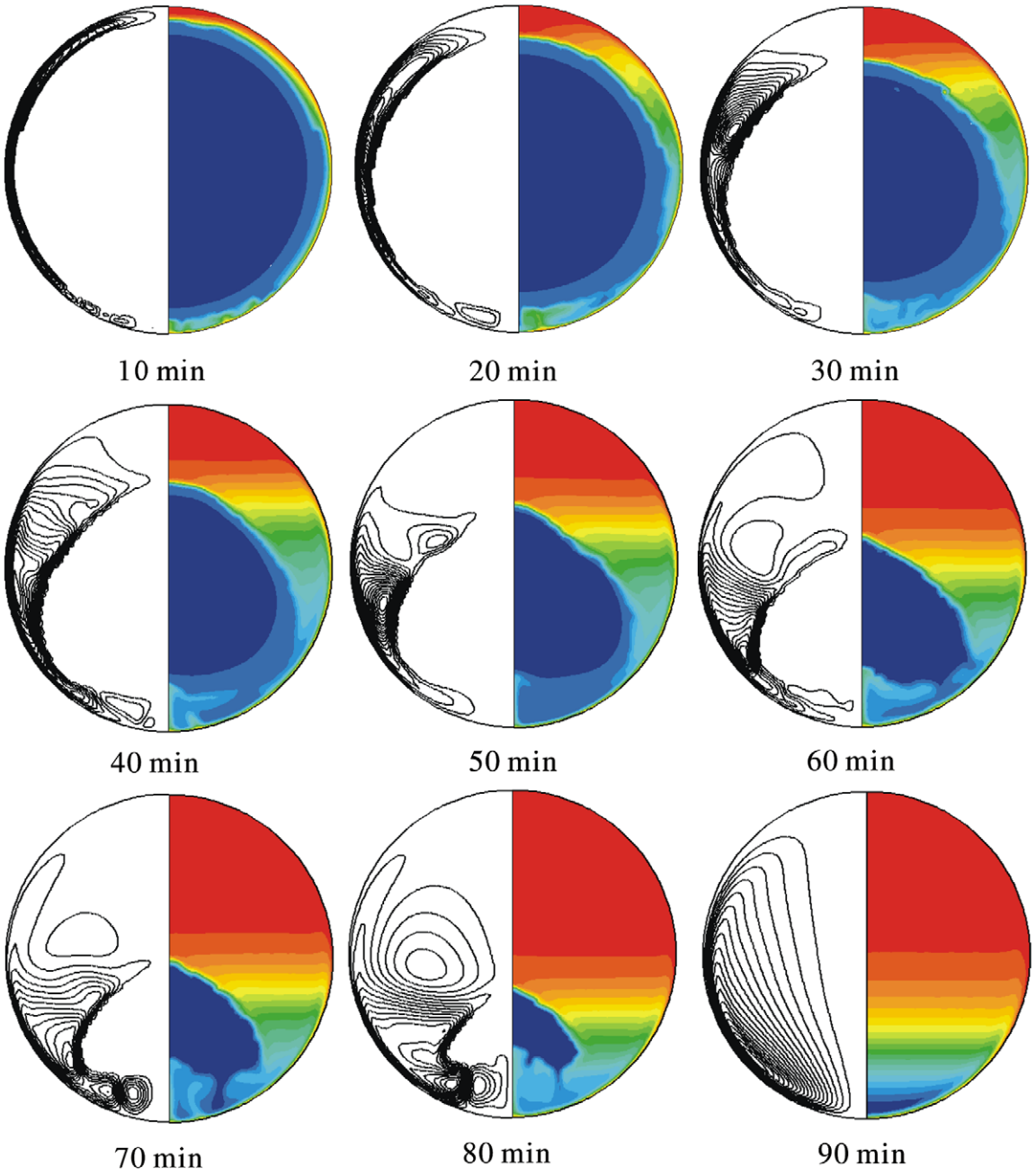

Fig. 3. Computed streamlines and temperature contours at 10 min intervals.

3.3. Comparison of the experimental temperature data to computed predictions

The novelty of the present paper lies in the availability of detailed temperature data that were collected during the course of the melting process along the vertical diameter of the sphere and comparison of this information to results of CFD simulations. The order of the comparisons will be based on when the solid–liquid interface passed over a thermocouple. Based on the measured thermocouple data, these were locations A, H, G, B, F, E, C, and D (Fig. 1). The locations of these measurement points along with the measured and computed instants at which phase change occurred at those points are summarized in Table 2.

The time-dependent variations of the measured temperature readings and computed predictions at point A that is located a distance of 44 mm below the center of the sphere is given in Fig. 5. Point A is the nearest thermocouple to the bottom of the sphere and was the first measurement location at which the thermocouple reading sensed the motion of the solid–liquid interface. Even though the temperature readings were sampled at shorter intervals, only selected measured data are shown by the solid square symbols, whereas the computed predictions are shown as solid lines. The chaotic convective motion that is expected in the thin unstable layer between point A and the inner wall of the sphere is clearly registered by the thermocouple readings and also exhibited by the temperature predictions starting at about 16 min. The persistence of the unstable liquid layer and the ensuing chaotic temperature readings are observed until about 94th minute after which there is no more solid left in the capsule.

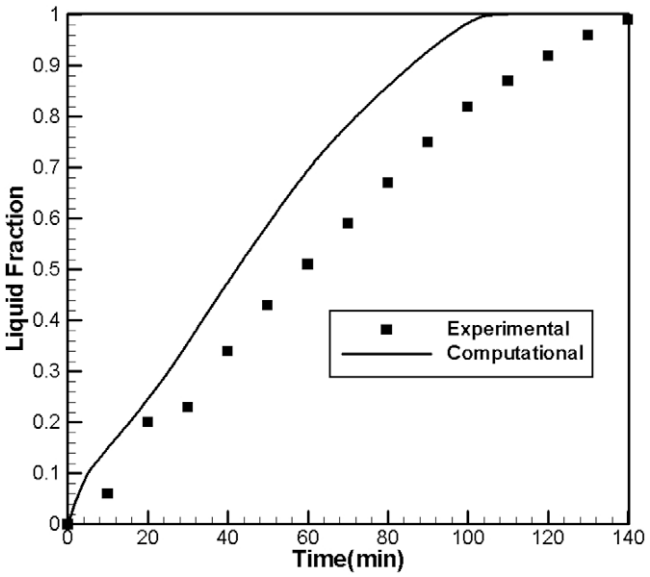

Fig. 4. Time-dependent variations of the liquid fractions determined computationally and experimentally.

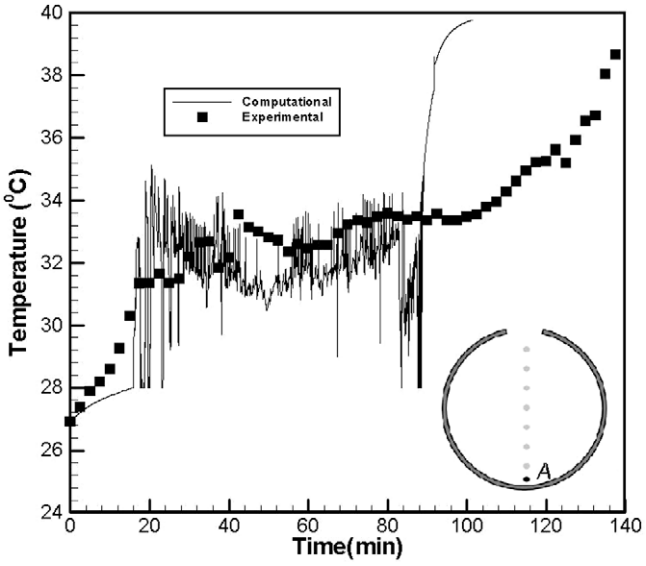

Fig. 5. Comparison of the computed and measured temperatures at point A at a distance of 0.433 diameters below the center.

A very interesting feature of phase change and the ensuing natural convection in a spherical capsule is the simultaneous existence of thermally stable and unstable fluid layers in the vicinity of the symmetry axis. This is illustrated schematically in Fig. 6 that shows enlarged views of these two fluid layers. At the given instant shown (50 min), for the greater portion of the symmetry axis above the center, horizontal stratified fluid layers are observed with the hot lighter fluid sitting on top of cooler dense layers. Such a system is denoted to be thermally stable, where fluid motion is negligible and heat conduction dominates. In contrast, the portion of the symmetry axis between the solid PCM's wavy bottom and the bottom of the sphere is composed of cold fluid layers on top of hotter dense layers. This type of system is denoted to be thermally unstable and will feature recirculating cells. One can clearly observe the vertical rising of a hot column of liquid away from the bottom wall toward the wavy

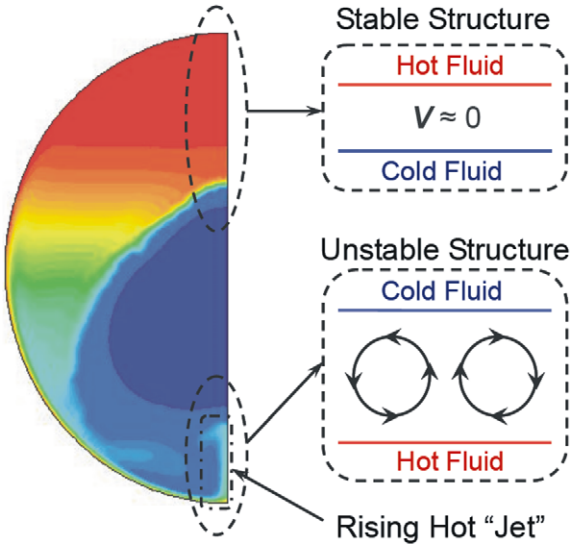

Fig. 6. Thermally stable and unstable layer structures along the symmetry axis.

bottom surface of the solid PCM in Fig. 6. Similar findings were also observed by the authors [25] who studied natural convection within a sphere container. Establishment of unstable layers and the ensuing chaotic convection have also been observed in melting of PCM within cylindrical tubes [19,20,26]. The waviness of the bottom part of the PCM and expedited melting due to penetration of multi-cellular roll structures were clearly observed in those studies. As for the comparison of the measured and computed temperature values in the stable layer near the top of the sphere, points H and G were the next locations on the thermocouple rake where the movement of the solid–liquid interface was registered. The comparison of the measured and computed temperature values at point G is presented in Fig. 7. The predicted temperature values closely match the experimental data followed by the dramatic rise of temperature upon melting. However, due to the stable nature of the liquid layer that contains both points G and H, no strong convective motion that would cause chaotic

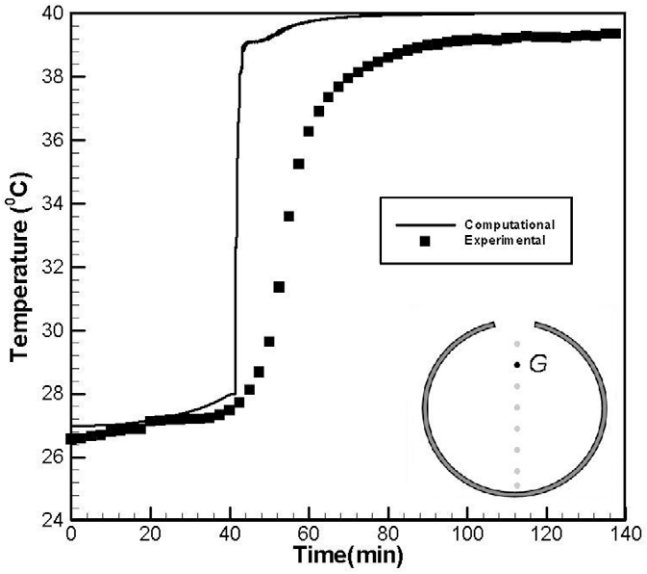

Fig. 7. Comparison of the computed and measured temperatures at point G at a distance of 0.246 diameters above the center.

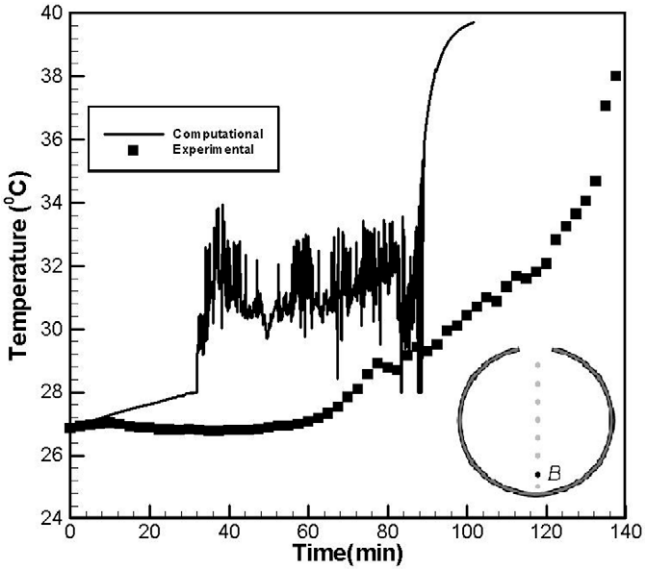

Fig. 8. Comparison of the computed and measured temperatures at point B at a distance of 0.369 diameters below the center.

temperature readings are registered. A similar figure was obtained at point H that is the location of the highest thermocouple within the sphere but it is not shown due to its close resemblance to Fig. 7.

The time-dependent variations of the measured temperature readings and computed predictions at point B that is located a distance of 37.5 mm below the center of the sphere is given in Fig. 8. Point B is positioned above point A along the vertical symmetry axis within the evolving unstable fluid layer. The thermocouple readings at this point were not as disorderly as those for point A in Fig. 5 whereas the numerical predictions suggest temperature oscillations between 28 and 34 °C limits. The predictions of the temperature variation along with the thermocouple measurements at point D are presented in Fig. 9. This point is located 12.5 mm below the center of the sphere and was the last point at which the thermocouple reading started to go above the melting temperature

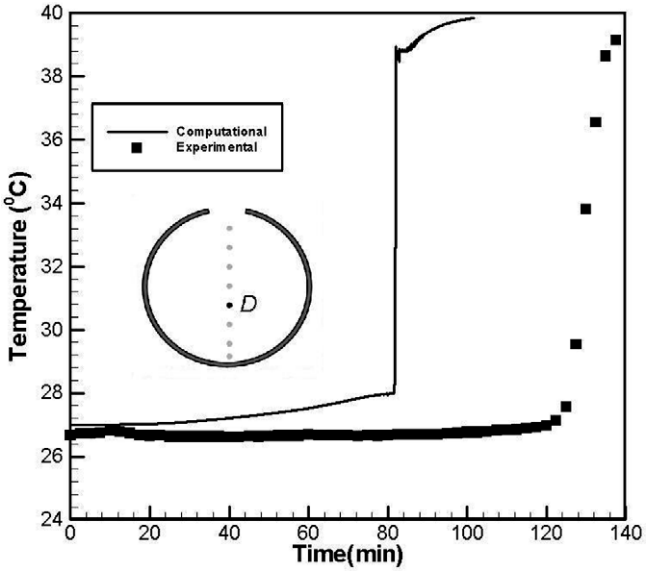

Fig. 9. Comparison of the computed and measured temperatures at point D at a distance of 0.123 diameters below the center.

of the PCM. The instant of phase change is predicted to take place about 40 min earlier that the collected temperature data. Upon melting, the predicted temperature values at point D exhibit very weak fluctuations. By this time, the inner section of the spherical container is fully stratified and convective fluid motion is not supported by the prevailing stable flow system.

Comparing the temperature measurements at points C–H to computed results, it was clearly observed that the deviation between the time instants at which the interface passed over those locations increased with the distance away from the bottom of the capsule. Specifically, at point H near the top, this deviation was 2 min, whereas at point C near the bottom, this deviation was 38 min (Table 2). This disparity can be linked to the thermal stratification within the "constant temperature bath" that encloses the capsule. This possibility is discussed in the next section.

3.4. Sources of discrepancies between experimental observations and numerical predictions

Overall, the general trends of the melting process are predicted well, however the quantitative data on the melting instants at the monitored points and instantaneous liquid volume fraction show discrepancies. Specifically, the computational results suggest a faster melting rate and a very pronounced unstable flow structure at the bottom of the sphere. We will not comment on advantages or shortcomings of the phase change model for this system. This is because the melting problem in a sphere is a complicated arrangement for benchmarking purposes in comparison to a differentially-heated set-up that was studied exhaustively by the authors [27]. Instead, we focus on three other concerns and draw attention to those issues.

Firstly, the experimentally-observed waviness of the bottom of the solid PCM in comparison to predictions that suggested more intense melting due to the unstable nature of the liquid layer points to the possible influence of a base support that was used to hold the sphere in position. Presence of a cylinder support with a diameter equal to about 0.375 diameters of the sphere was clearly visible in photographs shown in [17]. This arrangement could have easily lowered flow of heat through the bottom wall of the sphere. This in turn, would have brought about longer melting periods and weakened the intensity of the unstable thermal layer that is responsible for the waviness and intense melting of the bottom surface of the solid PCM.

The thermal state of the perceived "constant temperature bath" and its influence on the observed discrepancies is another area of concern. Thermal stratification due to buoyancy-driven convection is unavoidable in containers [24,25] and in the present case, it can become more complicated upon introduction of forced convection in form of inlet and outlet ports, e.g. [28]. In the present set-up, we suspect that thermal stratification within the "constant temperature bath" might have played a big role establishing a height-dependent variation of heat flux into the sphere. The presence of hotter fluid in the upper part of the bath could have easily been the reason for the expedited melting within the top half of the sphere. The systematic and increasing deviation of the computed results and thermocouple measurements as one moves lower into the sphere and away from the top supports this observation. The present simulations were not set up to account for such complications of the thermal state outside the sphere. It is suggested that researchers should consider the coupled modeling of the test-section and the enclosing bath in their future studies.

Finally, intrusiveness of the thermocouple measurements needs to be mentioned. In addition to disturbing the three-dimensional unstable layer, the difficulty associated with knowing the exact positions of the thermocouples could have contributed to the strict

matching of the experimental data to the computational simulations.

4. Conclusions

Based on the findings of the present experimental/computational study of the constrained melting within a spherical capsule, the following conclusions are drawn:

1. Through visualization of the melting process, it is observed that conductive heat transfer dominates during the early period, as evident by the near-spherical shape of the PCM. As buoyancy-driven convection is strengthened due to the growth of the melt zone, it is observed that melting in the top region of the sphere is much faster than in the bottom region of the sphere. Waviness of the bottom surface of the PCM was also observed.
2. The findings of the visualization study are substantiated by the computational results that show strong thermal stratification of the molten liquid in the upper half of the sphere. This is due to rising of the molten liquid along the inner surface of the sphere that replaces the colder fluid. The waviness and excessive melting of the bottom of the PCM is shown to be under-estimated by the experimental observation. This discrepancy is linked to the use of a support structure to hold the sphere that could have inhibited heat from reaching the bottom of the sphere.
3. The measured temperature data at the bottom of the sphere clearly show the establishment of an unstable fluid layer that supports chaotic fluctuations and is responsible for waviness of the bottom of the PCM. Computational results closely match the thermocouple readings at the bottom of the sphere and clearly predict a chaotic flow structure.
4. The comparison between the computed and measured temperatures in the top half of the sphere point to the stable nature of the molten liquid layer in that zone. The computational results start to deviate from the measured temperature readings further and further, as one considers thermocouples moving lower from the top of the sphere. This systematic delay in prediction of the melting instant is linked to the thermal stratification within the "constant temperature bath" that encloses the capsule.

Acknowledgements

The second author (SFH), at that time a Ph.D.-candidate in Aerospace Engineering at the Sharif University of Technology, acknowledges the support of the Ministry of Science, Research and Technology of the I. R. Iran through availability of a short-term scholarship to conduct research at Auburn University.

References

[1] P.B. Grimado, B.A. Boley, A numerical solution for the symmetric melting of spheres, Int. J. Numer. Meth. Eng. 2 (1970) 175–188.
[2] F.E. Moore, Y. Bayazitoglu, Melting within a spherical enclosure, J. Heat Transfer 104 (1982) 19–23.
[3] P.A. Bahrami, T.G. Wang, Analysis of gravity and conduction-driven melting in a sphere, J. Heat Transfer 109 (1987) 806–809.
[4] S.K. Roy, S. Sengupta, The melting process in spherical enclosures, J. Heat Transfer 109 (1987) 460–462.
[5] S.K. Roy, S. Sengupta, Melting of a free solid in a spherical enclosure: effects of subcooling, J. Solar Energy Eng. 111 (1989) 32–36.
[6] S.K. Roy, S. Sengupta, Gravity-assisted melting in a spherical enclosure: effects of natural convection, Int. J. Heat Mass Transfer 33 (1990) 1135–1147.
[7] S.A. Fomin, T.S. Saitoh, Melting of unfixed material in spherical capsule with non-isothermal wall, Int. J. Heat Mass Transfer 42 (1999) 4197–4205.
[8] K. Cho, S.H. Choi, Thermal characteristics of paraffin in a spherical capsule during freezing and melting processes, Int. J. Heat Mass Transfer 43 (2000) 3183–3196.
[9] J.M. Khodadadi, Y. Zhang, Effects of buoyancy-driven convection on melting within spherical containers, Int. J. Heat Mass Transfer 44 (2001) 1605–1618.
[10] I.W. Eames, K.T. Adref, Freezing and melting of water in spherical enclosures of the type used in thermal (ice) storage systems, Appl. Therm. Eng. 22 (2002) 733–745.
[11] K.T. Adref, I.W. Eames, Experiment on charging and discharging of spherical thermal (ice) storage elements, Int. J. Energy Res. 26 (2002) 949–964.
[12] K.A.R. Ismail, J.R. Henriques, T.M. da Silva, A parametric study on ice formation inside a spherical capsule, Int. J. Therm. Sci. 42 (2003) 881–887.
[13] H. Koizumi, Time and spatial heat transfer performance around an isothermally heated sphere placed in a uniform downwardly directed flow (in relation to the enhancement of latent heat storage rate in a spherical capsule), Appl. Therm. Eng. 24 (2004) 2583–2600.
[14] H. Ettouney, H. El-Dessouky, A. Al-Ali, Heat transfer during phase change of paraffin wax stored in spherical shells, J. Solar Energy Eng. 127 (2005) 357–365.
[15] A.F. Regin, S.C. Solanki, J.S. Saini, Experimental and numerical analysis of melting of PCM inside a spherical capsule, in: Proc. of the 9th AIAA/ASME Joint Thermophysics and Heat Transfer Conference (CD ROM), Paper AIAA 2006-3618, San Francisco, CA, 2006, 12 pp.
[16] E. Assis, L. Katsman, G. Ziskind, R. Letan, Numerical and experimental study of melting in a spherical shell, Int. J. Heat Mass Transfer 50 (2007) 1790–1804.
[17] F.L. Tan, Constrained and unconstrained melting inside a sphere, Int. Comm. Heat Mass Transfer 35 (2008) 466–475.
[18] W. Chen, Y.S. Zhao, L. Luo, F. Sun, Unified formulation for contact melting inside a symmetric enclosure, J. Thermophys. Heat Transfer 22 (2008) 227–233.
[19] T. Saitoh, K. Hirose, High Rayleigh number solutions to problems of latent heat thermal energy storage in a horizontal cylinder capsule, J. Heat Transfer 104 (1982) 545–553.
[20] H. Rieger, U. Projahn, M. Bareiss, H. Beer, Heat transfer during melting inside a horizontal tube, J. Heat Transfer 105 (1983) 226–234.
[21] V.R. Voller, C. Prakash, A fixed grid numerical modelling methodology for convection–diffusion mushy region phase-change problems, Int. J. Heat Mass Transfer 30 (1987) 1709–1719.
[22] S.V. Patankar, Numerical Heat Transfer and Fluid Flow, Hemisphere, Washington, DC, 1980.
[23] FLUENT 6.1 User's Guide, Fluent Inc., Lebanon, NH, 2003.
[24] Y. Zhang, J.M. Khodadadi, F. Shen, Pseudosteady-state natural convection inside spherical containers partially filled with a porous medium, Int. J. Heat Mass Transfer 42 (2000) 2327–2336.
[25] Y. Duan, S.F. Hosseinizadeh, J.M. Khodadadi, Effect of an insulated baffle on pseudosteady-state natural convection inside spherical containers, in: Proc. of the 2007 ASME–JSME Thermal Engineering Summer Heat Transfer Conference (CD ROM), Paper HT 2007-32340, Vancouver, BC, Canada, 2007, 10 pp.
[26] J.D. Chung, C.-J. Kim, H. Yoo, J.S. Lee, Numerical investigation on the bifurcative natural convection in a horizontal concentric annulus, Numer. Heat Transfer, Part A 36 (1999) 291–307.
[27] J.M. Khodadadi, S.F. Hosseinizadeh, Nanoparticle-enhanced phase change materials (NEPCM) with great potential for improved thermal energy storage, Int. Comm. Heat Mass Transfer 34 (2007) 534–543.
[28] S.M. Saeidi, J.M. Khodadadi, Forced convection in a square cavity with inlet and outlet ports, Int. J. Heat Mass Transfer 49 (2006) 1896–1906.